Cation mono and co doped anatase TiO2 nanotubes: an ab initio investigation of electronic and optical properties

Mohamed Mostafa Fadlallah, Ulrich Eckern

Cation Mono- and Co-Doped Anatase TiO$_2$ Nanotubes: An Ab Initio Investigation of Electronic and Optical Properties

Mohamed M. Fadlallah* and Ulrich Eckern*

The structural, electronic, and optical properties of metal (Si, Ge, Sn, and Pb) mono- and co-doped anatase TiO$_2$ nanotubes are investigated, to elucidate their potential for photocatalytic applications. It is found that Si-doped TiO$_2$ nanotubes are more stable than those doped with Ge, Sn, or Pb. All dopants lower the bandgap, except the (Ge, Sn) co-doped structure, the decrease depending on the concentration and the type of dopant. Correspondingly, a redshift in the optical properties for all kinds of dopings is obtained. Even though a Pb mono- and co-doped TiO$_2$ nanotube has the lowest bandgap, these systems are not suitable for water splitting, due to the location of the conduction band edges, in contrast to Si, Ge, and Sn mono-doped TiO$_2$ nanotubes. On the other hand, co-doping of TiO$_2$ does not improve its photocatalytic properties. The findings are consistent with recent experiments, which show an enhancement of light absorption for Si- and Sn-doped TiO$_2$ nanotubes.

1. Introduction

Titanium dioxide (TiO$_2$), also known as titania, has been widely studied as a promising material for many applications because of its low production cost, chemical stability, and nontoxicity.[1–3] Titania is useful for, in particular, solar cells,[4] batteries,[5] photochemical[6] and photocatalytic[7] applications, gas sensing,[8] and hydrogen storage.[9–11] However, TiO$_2$ can only be activated by ultraviolet light due to its large bandgap (3.0 eV for the rutile and 3.2 eV for the anatase phase). Therefore, engineering the bandgap[12,13] of titania (the term "bandgap engineering," introduced more than 30 years ago, generally refers to all attempts at modifying the bandgap, e.g., by heterostructuring, combining

suitable materials, and doping) to increase its photosensitivity for visible light is a major target in photocatalyst studies.

In recent years, various low-dimensional TiO$_2$ nanostructures have been prepared, such as thin films,[14] nanoparticles,[15,16] nanowires,[17,18] and nanotubes.[19,20] TiO$_2$ nanotube (TNT) arrays are most interesting for applications due to their large internal surface and highly ordered geometry.[21–23] The structural properties, stability, and electronic structure of different TNT structures (anatase and lepidocrocite) have been discussed, e.g., in the previous study.[24] All anatase nanotubes are semiconductors with direct bandgaps, whereas the lepidocrocite nanotubes are semiconductors with indirect gaps. In addition, anatase nanotubes were found to be most stable; their stability increases with increasing diameter.[25–27] The rolling of an anatase (101) sheet along the [101] and [010] directions has been used to build (n,0) and (0,n) TNTs, respectively.[28] Further details of the geometrical properties of TNTs, in particular, about the folding procedure and the anatase layer basic translation vectors, can be found in the previous studies.[24–28]

The experimental results show that the predominant peaks of anatase and rutile nanotubes are (101) and (110).[29,30] Recently, several mono- and co-doped TNTs have been synthesized, e.g., C,[31] P,[32] Co,[33] Si,[34] and Sn[35] mono-doped, as well as (C/N, F) co-doped[36] TNTs. On the other hand, doped TNTs have been studied theoretically only occasionally, e.g., N and B doping,[37] C, N, S, and Fe doping,[38] (N, S) co-doping,[39] and nonmetal and halogen doping.[40]

In the context of this study, we note that an improvement of the photocatalytic properties of bulk TiO$_2$ has been observed experimentally[41,42] and calculated theoretically[43,44] for Si doping. Other dopings (Ge, Sn, and Pb) are also known to reduce the bandgap in the rutile bulk system, whereas Sn and Pb dopings slightly broaden the bandgap in anatase TiO$_2$.[43] Experimentally, an improvement of photocatalytic properties was found for Sn-doped bulk systems synthesized by the hydrothermal method.[45] TiO$_2$ thin films doped with Si,[46] Sn,[47] Pb,[48] and Ge[49] have been prepared and investigated, generally showing an improvement of photocatalytic activity upon doping. With respect to TNT, a suitable doping with Si also improves the light absorption.[34,50] Similar results have been found for Sn doping where, however, also a transformation from anatase to rutile is observed.[35] Thus, in the light of these previous experimental and theoretical studies, and in view of their potential high relevance for photocatalytic applications, we perform a

Prof. M. M. Fadlallah
Physics Department
Faculty of Science
Benha University
13518 Benha, Qalubiya Governorate, Egypt
E-mail: mohamed.fadlallah@fsc.bu.edu.eg

Prof. U. Eckern
Institute of Physics
University of Augsburg
86135 Augsburg, Germany
E-mail: ulrich.eckern@physik.uni-augsburg.de

The ORCID identification number(s) for the author(s) of this article can be found under https://doi.org/10.1002/pssb.201900217.

ADVANCED
SCIENCE NEWS
www.advancedsciencenews.com

physica
pss status solidi b
www.pss-b.com

systematic study of doping anatase TNT with group-IV elements, as a function of dopant concentrations; in addition, co-doping effects are also investigated. Our focus in this work is on the anatase nanotube because the TiO_2 anatase (101) surface is known to be a quite effective surface for solar cell applications.[51]

In the following, we investigate the effect of the mono-dopants (Si, Ge, Sn, and Pb) on the structure and stability of anatase phase (8,0) titania nanotubes (TNTs) (Section 2). Then, we study the electronic structure of doped TNTs (Section 3), followed by a discussion of the optical properties (Section 4). An application of this study is the splitting of water (Section 5). We close our work with a brief summary (Section 6). The computational details are given in the final section (Section 7).

2. Optimized Structure and Stability

The total number of the atoms in the unit cell of a TNT is related to the number of atoms in one unit cell (48 atoms) in the surface layer. We use a supercell including two TNT unit cells to study the effect of changing the doping concentration. **Figure 1** shows the structure of two unit cells of (8,0) TNT. The fundamental periodic of the TNT nanotube (along z direction) is found to be 10.49 Å, which is only slightly larger than the value obtained in a previous study, 10.13 Å.[27] In that paper, only one unit cell was studied, whose length was determined to be 5.065 Å; hence, we compare with twice this value. No symmetry was preserved during structure optimization. Concerning other geometric parameters, we find the inner diameter of the nanotube (see the

lower part of Figure 1), i.e., between an O3 and its opposite counterpart, to be given by 7.07 Å, whereas the distance between an O1 and its opposite counterpart is 12.05 Å; the diameter with respect to the Ti atoms is 9.51 Å, and the O1–O3 distance is 2.49 Å. The bond length Ti1–O1 (equal to Ti1–O3) is 1.84 Å, whereas the bond Ti2–O2 is slightly longer, 1.95 Å, in good agreement with previous works.[27,52]

Cation doping of the TNT is introduced by replacing Ti atoms by the dopants. Replacing one Ti by a metal dopant corresponds to ≈1.0% dopant concentration. If two atoms are substituted, the doping concentrations will double, and so on. These dopant concentrations are comparable to those reported experimentally.[53] Though there are several possible dopant locations for 2% and 3% doping, we have opted, in this work, for configurations in which the dopants are as far apart as possible, namely, 9.8 Å for 2%, and 9.8, 9.3, and 7.4 Å for 3% concentrations, thereby avoiding as much as possible any dopant–dopant interaction. With this choice, we also avoid major distortions of the nanotube's structure. Naturally, we thus exclude the possibility of dopant cluster formation (which could be an interesting question in itself,[54] but is beyond the scope of this study).

The optimized average bond lengths around the dopant atoms are listed in **Table 1**. The bond length between the dopant atom and the O atom increases as the ionic radius of the dopant increases: Si, Ge, Sn, and Pb, with radii 0.40, 0.53, 0.69, and 1.19 Å, respectively. In comparison, the ionic radius of Ti^{4+} is 0.61 Å.

The charge deficiency on the metal, estimated as the difference between electronic charge densities obtained with the Mulliken population analysis, is also given in Table 1. The table
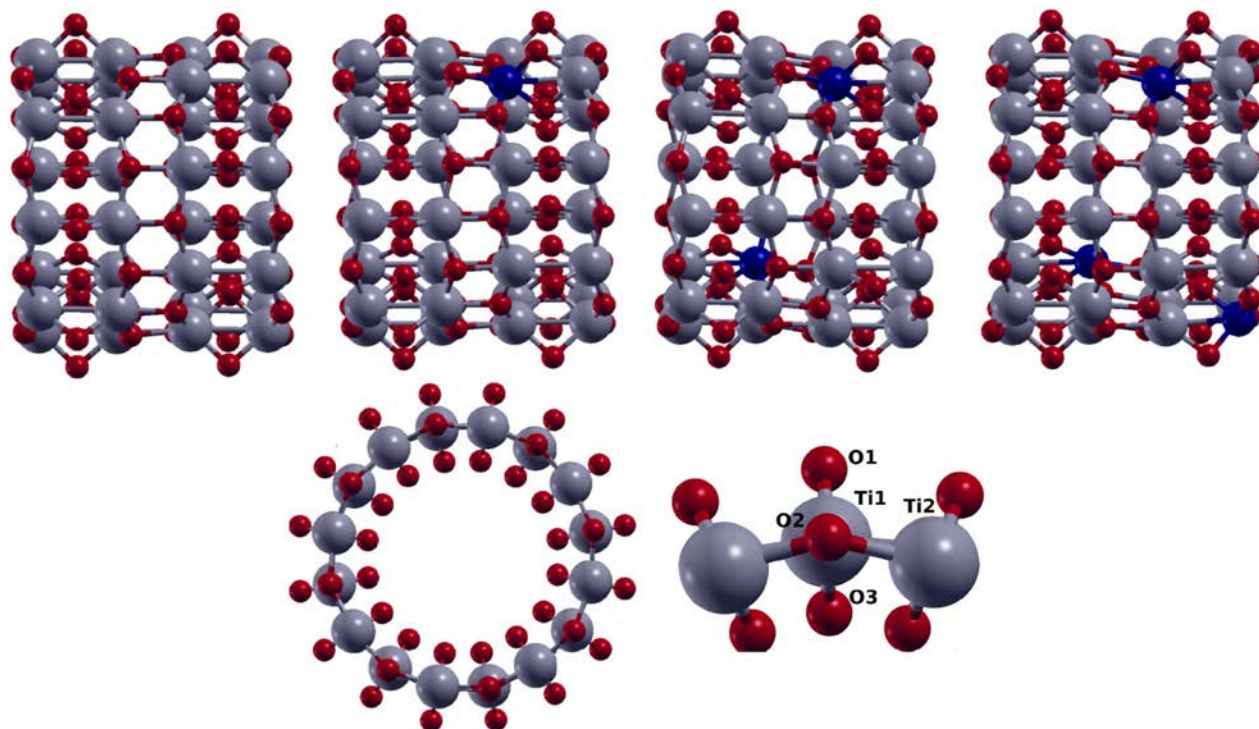

Figure 1. Top part: Optimal configuration (side view) for pristine TNT, 1% doped TNT, 2% doped TNT, and 3% doped TNT (from left to right). Lower part: Top view of the pristine TNT (left) and detail of the wall (right). The indicated labels are discussed in the main text. Red, grey, and blue spheres represent O, Ti, and dopant atoms, respectively.

Table 1. Bond lengths between dopant metal and oxygen, M–O (Å), Mulliken charge on dopants (e), and formation energy, E_{form} (eV), for doped TNT.

Metal	Si	Ge	Sn	Pb
M–O	1.77	1.94	2.09	2.18
Mulliken charge	2.12	1.48	2.05	1.78
E_{form}	1.5	2.1	3.1	4.2

shows that the charge transfer from the dopant atom to the surrounding O atom is rather high for Si and Sn, as compared with Ge and Pb. The formation energy of doped TNTs is used to investigate the stability of the structures. The formation energy (E_{form}) of the dopant atoms can be calculated as follows[55]

$$E_{form} = E_{M-TiO_2} + \mu_{Ti} - (E_{TiO_2} + \mu_M) \qquad (1)$$

where E_{M-TiO_2} and E_{TiO_2} are the total energies of the metal-doped TiO_2 and the pristine TNT, respectively, whereas μ_{Ti} and μ_M denote the chemical potentials for Ti and the dopant; the latter is assumed to be equal to the energy of one atom in its corresponding bulk structure.

The formation energy depends on the growth conditions, which can be Ti-rich or O-rich.[56] For the Ti-rich condition, thermodynamic equilibrium is assumed for the Ti bulk solid phase; thus, its chemical potential is fixed at μ_{Ti}, whereas the chemical potential of O is fixed by the growth conditions. Under the O-rich condition, O is assumed to be in equilibrium with O_2 molecules; thus, the chemical potential of O is $\mu_O = \mu_{O_2}/2$. We present the formation energy under the O-rich condition, which is lower than for the Ti-rich condition. The stability of nanotubes with dopants is in the following order: Si, Ge, Sn, and Pb. The behavior of the formation energies can be understood, to a large extent, in terms of the dopant's electronegativity (see also Section 5) given by 1.90 (Si), 2.01 (Ge), 1.96 (Sn), and 2.33 (Pb) (Pauling scale). On the one hand, one note that the formation energy of Si is smaller than that of the other dopants, corresponding to the fact that Si has the smallest

electronegativity. On the other hand, the Pb formation energy is the largest, and so is its electronegativity. From this point of view, Ge- and Sn-doped TNTs are "out of order," which can be related to the effect of electronegativity on the ionic radius, implying that the formation of Sn–O bonds is more favorable than Ge–O bonds. This behavior of formation energies and bond lengths is very similar to the behavior of the corresponding dopant in bulk TiO_2.[43]

3. Electronic Structure

In this section, we discuss the density of states (DOS) and the partial density of states (PDOS) for the doped TNTs under consideration, in particular, the behavior of the valence bands (VBs) and the conduction bands (CBs) upon doping, with focus on the modifications of the energy gap. To present the results in a concise and systematic fashion, we have chosen to measure the energy in the DOS and PDOS plots (Figure 2–6) relative to the top of the valence band energy, E_{TVB}, of the pristine TNT. For water splitting applications, on the other hand, the absolute energies are required, see Section 5.

Before going into detail, we emphasize that we have carefully checked the dependence of the results on the dopant positions. For example, for a concentration of 1%, we find that the total energy for different dopant positions varies only by less than 0.01 eV, and no change in the DOS is obtained. For 2% and 3% concentrations, we find that the stability increases upon increasing the distance between dopants. Hence, our calculations have been done at the largest possible distance(s) between dopant atoms.

Figure 2a shows the DOS for pristine TNTs (8,0). The calculated bandgap is 2.20 eV, which—as usual in density functional theory–generalized gradient approximation (DFT-GGA)—is lower than the corresponding experimental gap of the TNT (3.18–3.23 eV[57,58]). The Ti (3d) states dominate in the unoccupied states, whereas the O (2p) states contribute mostly to the occupied states with a minor contribution to the unoccupied states (see Figure 2b). The DOS and PDOS are very similar to the results obtained in the previous study.[52]
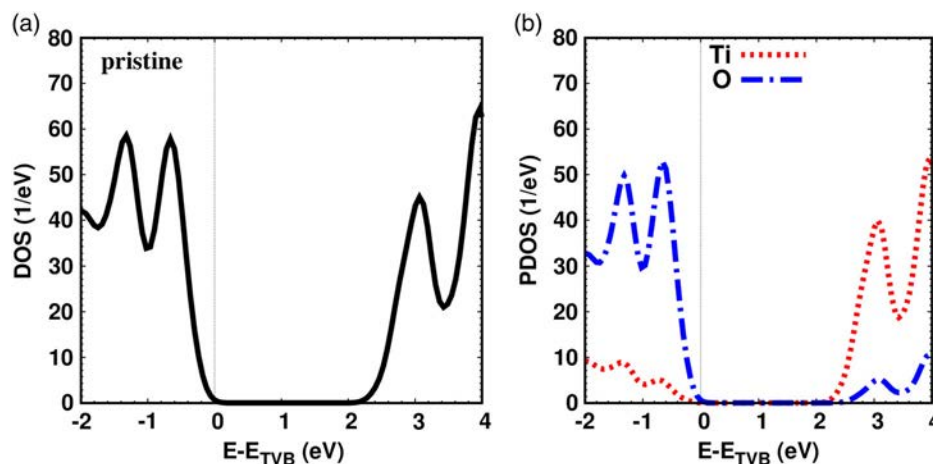

Figure 2. a) DOS and b) PDOS of the pristine TiO_2 (8,0) nanotube. The energy is given relative to the top of the valence band (TVB).

ADVANCED
SCIENCE NEWS
www.advancedsciencenews.com

physica
pssb
status
solidi

www.pss-b.com

3.1. Mono-Doped TNTs

3.1.1. Si Doping

The effect of Si doping at different concentrations on the electronic structure of TNT is shown in **Figure** 3b–d. The bandgap is 1.80 eV for 1% doping, less by 0.40 eV than that of the pristine TNT. The corresponding total DOS is similar to the pristine DOS, however, with a smaller bandgap (see the inset of Figure 3b as compared with Figure 2a). When the concentration increases to 2% and 3%, we find that the Si–Si distance decreases to 9.4 Å after optimization for 2% concentration, and to 9.4, 9.0, and 7.3 Å between different pairs of Si atoms for 3%. These values have to be compared with the original Ti–Ti distance of 9.8 Å for 2%, and 9.8, 9.3, and 7.4 Å for 3% concentrations. The bandgap remains at 1.80 eV for 2%, and increases to 1.86 eV for 3%. The computed bandgap reduction for the corresponding doped bulk system is found to be slightly smaller, 0.20 eV.[43] (In that paper, only 2% doping was studied.)

Concerning the detailed behavior, we note that on the scale of the figure an almost rigid, concentration independent downshift of about 1.3 eV of the VB is observed, accompanied by a slight "smearing" of the oscillations, which are visible below −0.5 eV in the pristine PDOS. The PDOS shows that the dopant states start contributing above 1 eV, with a distinct maximum at about 2.2 eV. The dopant contribution is rather small, but increases continuously with increasing concentration. Comparing with the Ti PDOS (Figure 3a), we realize that while the onset of Si states is clearly lower than the onset of the pristine Ti states, the latter coincides with the maximum of the Si PDOS. The evolution of the maximum of the Si PDOS can be seen more clearly in Figure 3b–d. It is located near 2.2 eV for 1% and 2% concentrations (Figure 3b,c), and then shifts downward to about 1.8 eV for 3% concentration (see Figure 3d). As the location of dopant states shifts closer to the CB edge, the bandgap increases. The decrease in the bandgap—as compared with the pristine TNT—is consistent with the observed increase in optical absorption of TNT upon Si doping.[34,50,59]
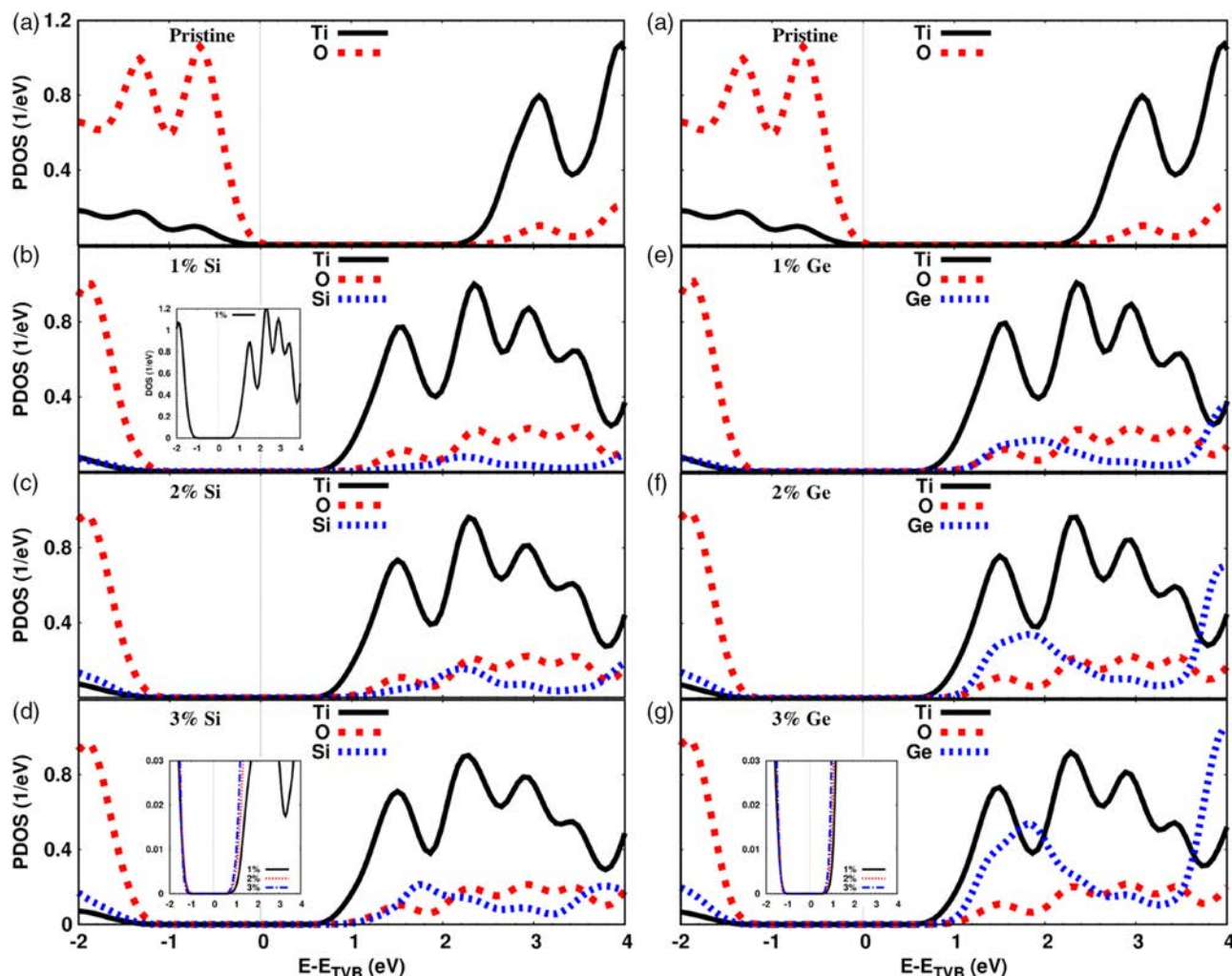

Figure 3. PDOS for a) pristine TNT (shown at the top of both columns), and mono-doping at different concentrations for b) 1%, c) 2%, and d) 3% Si, and for e) 1%, f) 2%, and g) 3% Ge. (Ti, O) states are scaled down by a factor of 50 to allow easy comparison. The energy is given relative to the TVB of the pristine TNT. The insets in (b), (d), and (g) show the corresponding total DOS (Si doping), and PDOS (Si, Ge) on an even more reduced scale.

3.1.2. Ge Doping

The optimized Ge–Ge distances are slightly larger than the Si–Si values, consistent with the increase in ionic radius, namely, 9.7 Å for 2% concentration (and hence only 0.1 Å smaller than the original Ti–Ti distance), and 9.7, 9.2, and 7.5 Å for 3% concentration. Figure 3e,g shows that the bandgap is 1.86 eV, at any concentration, which is less than the pristine bandgap but larger than that for Si doping TNT at 1% and 2% concentrations because the location of Ge states is closer to CB edge than the Si states at these concentrations. The bandgap does not depend on the concentration because the dopant states peak position (1.86 eV) is rigid (Figure 3d). The peak in the Ge PDOS can be attributed to the fact that the Ge ionic radius and electronegativity are only slightly different in comparison with Ti. The shifts of the VB and the CB are quite similar to the case of Si doping, even though the Ge states give a stronger contribution in the PDOS (Figure 3d). Accordingly, the DOS of the Ge-doped system at different concentrations is very similar to the DOS of

the Si-doped structures (see the inset of Figure 3b). Again, the bulk gap reduction was reported to be slightly smaller, only 0.15 eV[43] compared with the present 0.34 eV.

3.1.3. Sn Doping

For Sn-doped TNTs, we find that for 2% concentration, the Sn–Sn distance is 9.8 Å, which is the same as the original distance of Ti atoms. Regarding 3% concentration, the distances are 9.8, 9.6, and 7.6 Å, which are larger than original distances. **Figure 4**b shows that the contribution of Sn states at 1% concentration is similar to the Ge-doping structure at 2% in the energy range from −2.0 to 2.5 eV. The distinct peak appears at 1.8 eV, which is the same as for Si at 3% and Ge at any concentration. Hence, the bandgap also is 1.86 eV. When the Sn concentration increases, the distinct peak slightly shifts to higher energy (Figure 4b,c), which is in the opposite direction compared with Si doping with increasing concentration. The distinct peak is located at 2.0 eV, and we find the gap to be 1.83 eV. Due to the

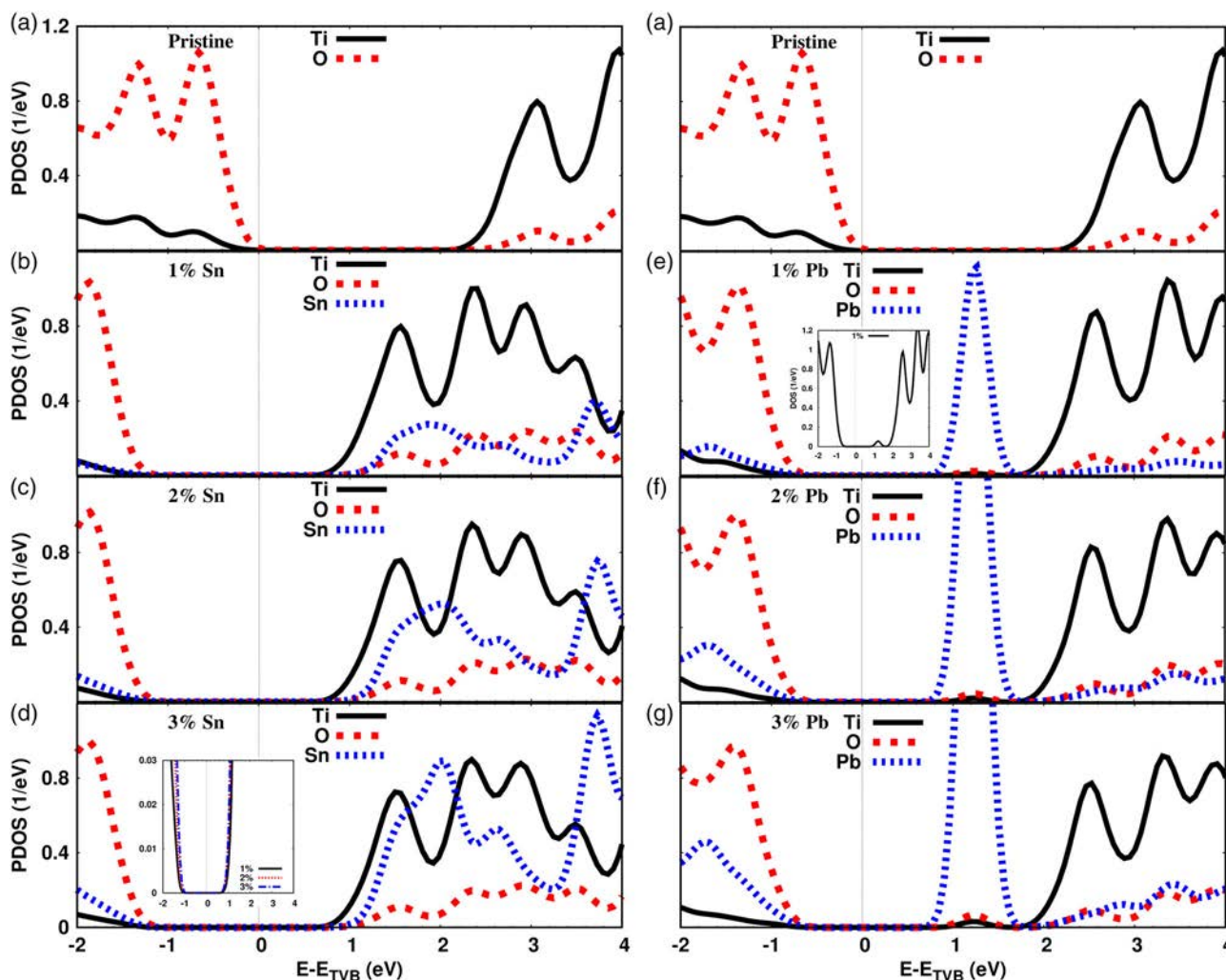**Figure 4.** PDOS for a) pristine TNT (shown at the top of both columns), and mono-doping at different concentrations for b) 1%, c) 2%, and d) 3% Sn, and for e) 1%, f) 2%, and g) 3% Pb. (Ti, O) states are scaled down by a factor of 50 to allow easy comparison. The energy is given relative to the TVB of the pristine TNT. The insets in (d) and (e) show the Sn PDOS on an even more reduced scale, as well as the total DOS (Pb doping).

similarity of the Ti PDOS of doped Sn structures with the corresponding one of Si-doped structures, the general behavior of the DOS for Sn doping is similar to the DOS for Si doping. The computed reduction of the bandgap through Sn doping also is in good agreement with the corresponding light absorption experiment.[35]

3.1.4. Pb Doping

Within the mono-doped series, we finally consider Pb. The optimized Pb–Pb distances are 10.0 Å for 2% concentration, and 10.0, 9.6, and 7.7 Å for 3% concentration. These values are larger than the original distances of the host atoms. The distinct peak of Pb states is not only located at a lower energy (1.2 eV) as compared with the peak of the previously discussed dopants, but also clearly lower than the Ti CB states (see Figure 4e–g), such that a separate dopant peak appears in the corresponding DOS. These states decrease the bandgap to 1.56 eV, which is the lowest bandgap in comparison with the other dopants at any concentration. On the other hand, the shift of the VB and CB edges is 0.5 and 0.3 eV, respectively, downward in energy, which is less than the corresponding values for the other systems. For the resulting DOS, see the inset of Figure 4e, as compared with the inset of Figure 3b. Increasing the concentration of Pb, the bandgap slightly decreases to 1.50 and 1.44 eV, for 2% and 3%, respectively. The PDOS shows that the majority of the additional states derive from the Pb states (see Figure 4f,g). The peak energy of the Pb states hardly changes with increasing doping.

To obtain a better understanding of the systematics of the aforementioned results, and of those presented in the following subsection, we emphasize that the relevant aspect is the energetic location of cation dopant states relative to the conduction band, in which the Ti $3d$ states dominate. In particular, we have been able to relate the characteristic concentration and dopant dependent shifts of the dopant PDOS, especially the distinct peak, to the behavior of the energy gap. In comparison with the doped bulk system,[43] we note, first of all, that the gap reduction for the doped TNT generally is stronger than in the bulk, where, in fact, a gap enhancement was found for 2% Sn or Pb doping. However, the stronger effect of doping—compared with the bulk system— appears reasonable because the disturbances created by dopants are expected to have a stronger influence in a reduced-dimensionality system such as a nanotube. With respect to the location of dopant states, we note that their respective peak energies obey the following inequality: $E_{Pb(6s)} < E_{Ti(3d)} < E_{Sn(5s)} < E_{Ge(4s)} < E_{Si(3s)}$. In particular, the Si, Ge, and Sn states are well within the conduction band, such that they are not able to form distinct dopant

states below the CB. Instead, they "only" reduce the energy gap. However, there is no obvious trend—except for the relation to the distinct dopant PDOS peak, as mentioned earlier—when the dopant concentration is increased (see **Table 2**): When the Si concentration is increased, the gap slightly increases, which likely can be related to the fact that a rather large geometric disturbance is created by Si, which has the smallest ionic radius, and that this disturbance is reduced upon doping, at least for 3%. While the gap for Ge doping is concentration independent, it is found to slightly decrease for Sn doping, which is reasonable because the ionic radius of Sn is larger than the ionic radius of Ti. However, these are rather subtle effects, and we believe it is hardly possible to identify a single "cause" for the systematics.

The only clear-cut case in the considered series is Pb, where the dopant states are strong and located in energy clearly below the conduction band. Thus, a separate peak in the DOS is formed, whose amplitude increases with dopant concentration. In addition, a strong reduction of the energy gap is found.

3.2. Co-Doped TNTs

Turning finally to co-doped TNTs, the doping concentration is 2% for two different substitutional atoms, and 3% for two atoms from the same kind plus one doping atom from another kind. We first study the effect of co-doping at 2%. Starting with Si–Ge, the optimized distance is 9.5 Å. This is approximately the average of the Si–Si and Ge–Ge distances at 2% concentration. **Figure 5**b shows the effect of (Si, Ge) co-doping on the electronic structure. The overlap between Si, Ge, and Ti states appears near the CB band; therefore, the bands shift to lower energy. This shift is less than the corresponding one in the case of 1% and 2% mono-doping with Si and Ge by 0.6 eV. The (Si, Ge) co-doped TNT has a bandgap of 1.92 eV, larger than the gap for Si and Ge mono-doping at any concentration. As we go down the group of dopants in the periodic table (4A), the dopant–dopant distance increases to 9.6 Å for Si–Sn and 9.7 Å for Si–Pb. The overlap between the dopant and the host atom states also increases slightly near the CB edge, so the bandgap of (Si, Sn) is 1.98 eV (see Figure 5c). Figure 5d shows the PDOS of the (Si, Pb) co-doped system, which is very similar to the DOS of the Pb mono-doped TNT. It is characterized by Pb dopant states below the conduction band. The bandgap for this co-doping is 1.50 eV, smaller than the gap of the 1% and equal to the 2% mono-doped Pb system.

As compared with the co-doped structures discussed earlier, the bands of (Ge, Sn) shift to higher energy, and the bandgap increases to 2.3 eV (Figure 5e), clearly larger than the gap of

Table 2. Calculated bandgap values (eV) for all concentrations and configurations considered; "pr" denotes the pristine TNT.

	pr	Si			Ge			Sn			Pb			Si/Ge		
		1%	2%	3%	1%	2%	3%	1%	2%	3%	1%	2%	3%	(1,1)	(2,1)	(1,2)
E_{gap}	2.20	1.80	1.80	1.86	1.86	1.86	1.86	1.86	1.83	1.83	1.56	1.50	1.44	1.92	1.92	1.92

	pr	Si/Sn			Si/Pb			Ge/Sn			Ge/Pb			Sn/Pb		
		(1,1)	(2,1)	(1,2)	(1,1)	(2,1)	(1,2)	(1,1)	(2,1)	(1,2)	(1,1)	(2,1)	(1,2)	(1,1)	(2,1)	(1,2)
E_{gap}	2.20	1.98	1.86	1.86	1.50	1.44	1.50	2.34	1.86	1.86	1.56	1.56	1.56	1.56	1.50	1.56

**ADVANCED
SCIENCE NEWS**

www.advancedsciencenews.com
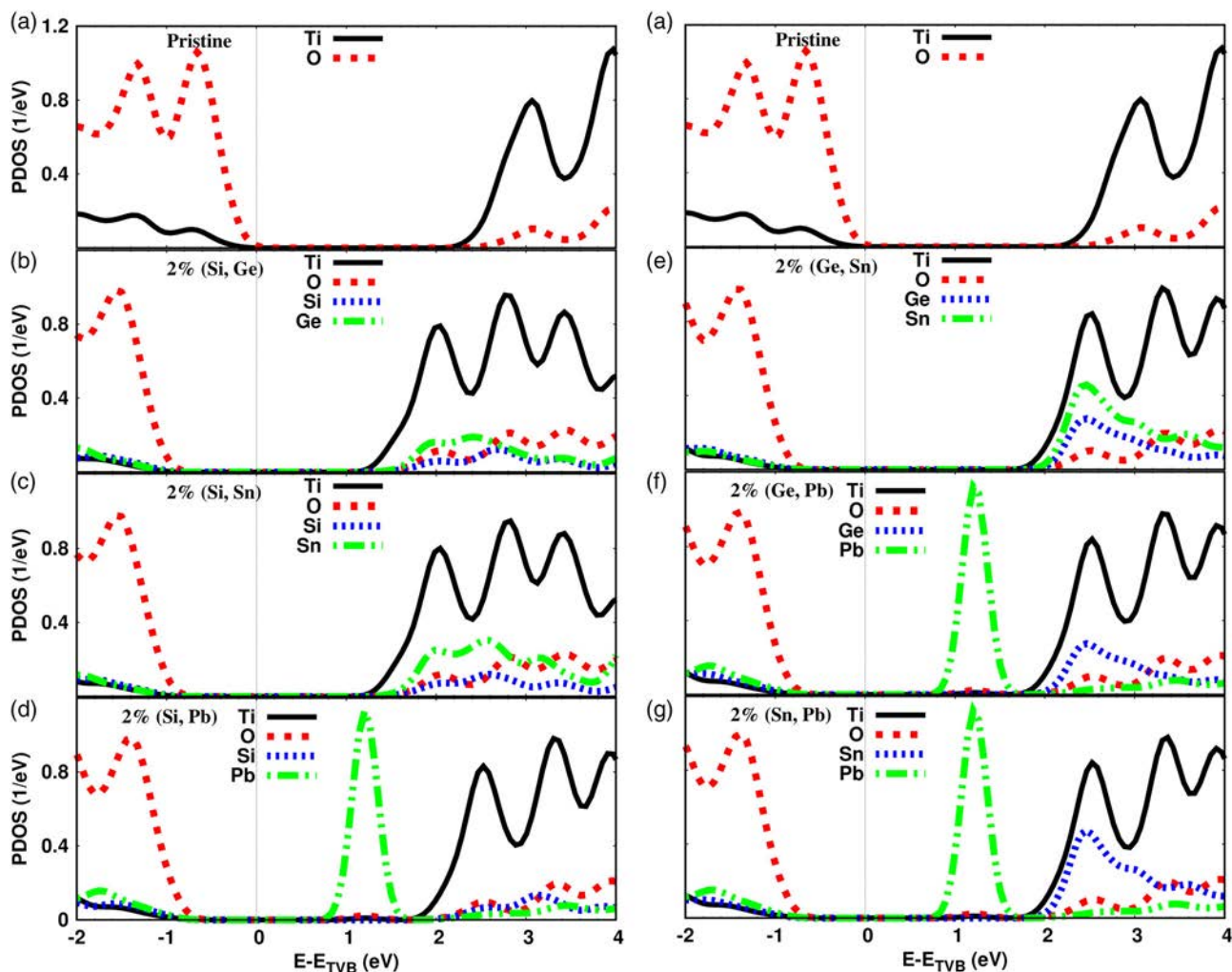
p s s b
physica status solidi

www.pss-b.com

Figure 5. PDOS for a) pristine TNT, and for 2% co-doping: b) (Si, Ge), c) (Si, Sn), d) (Si, Pb), e) (Ge, Sn), f) (Ge, Pb), and g) (Sn, Pb). The (Ti, O) states are scaled down by a factor of 50 to allow comparison. The energy is given relative to the TVB of the pristine TNT.

pristine TNT. The increase in the bandgap can be attributed to the strong interaction (bonding) between the dopant (such as Sn) and the Ti CB states in the energy range of 1.8–2.5 eV (see Figure 5e). The distance between Ge–Sn is similar to the Si–Sn distance (9.6 Å). If Sn is replaced by Pb, the distance of Ge–Pb increases to 9.8 Å, which is less than the Pb–Pb distance at 2%. Due to the interaction between Ge and Ti states near the CB edge, the Pb states slightly move toward higher energy, so the bandgap slightly increases to 1.56 eV as compared with (Si, Pb) (see Figure 5f). The last 2% co-doped system is (Sn, Pb) (Figure 5g) with 9.9 Å Sn–Pb distance. The distinct peak of the Sn dopant is located at the same position as for Ge (2.4 eV) (Figure 5c), and the Pb midgap states remain in their place; thus, the bandgap does not change. The bandgap of co-doped systems at 2% concentration is larger than the bandgap of the individual corresponding mono-doped structures because of good co-dopant states interactions near the CB edge, except for Pb doping. Table 2 summarizes the bandgap values of all structures considered.

At last, we study co-doped TNTs at high concentration, i.e., 3%. The distances in the (2Si, Ge) co-doped structure are

9.1 and 7.3 Å for Si–Ge and 9.4 Å for Si–Si, and for (Si, 2Ge) are 9.1 and 7.4 Å for Ge–Ge and 9.6 Å for Ge–Si. **Figure 6**b shows the PDOS of (2Si, Ge), which is practically identical to the (Si, Ge) case. Also, there is no change when another configuration (Si, 2Ge) is considered. The electronic structures of (Si, Ge)/(2Si, Ge)/(Si, 2Ge) co-dopants do not depend on the concentration of the individual dopants because all configurations have a similar effect at the same energy. Regarding (2Si, Sn), we find (see Figure 6c) that the overlap between states in the CB reduces the bandgap as compared with (Si, Sn) by ≈0.3 eV, and the gap becomes 1.86 eV, less than the bandgap of the same co-doped system at 2% concentration. The DOS of the (Si, 2Sn) system is practically the same as the (2Si, Sn) DOS, even though the distances differ slightly: 9.1 and 7.5 Å for Si–Sn and 9.8 Å for Si–Si for the former, and 9.2 and 7.4 Å for Si–Sn and 9.4 Å for Si–Si for the latter case.

For (2Si, Pb) co-doping (Figure 6d), the PDOSs show that the CB and Pb midgap states shift toward lower energy by 0.6 and 0.2 eV, respectively, as compared with the same co-doped system at low concentration (Figure 5d). This relatively strong shift in the CB is due to the shift of the corresponding Si states.
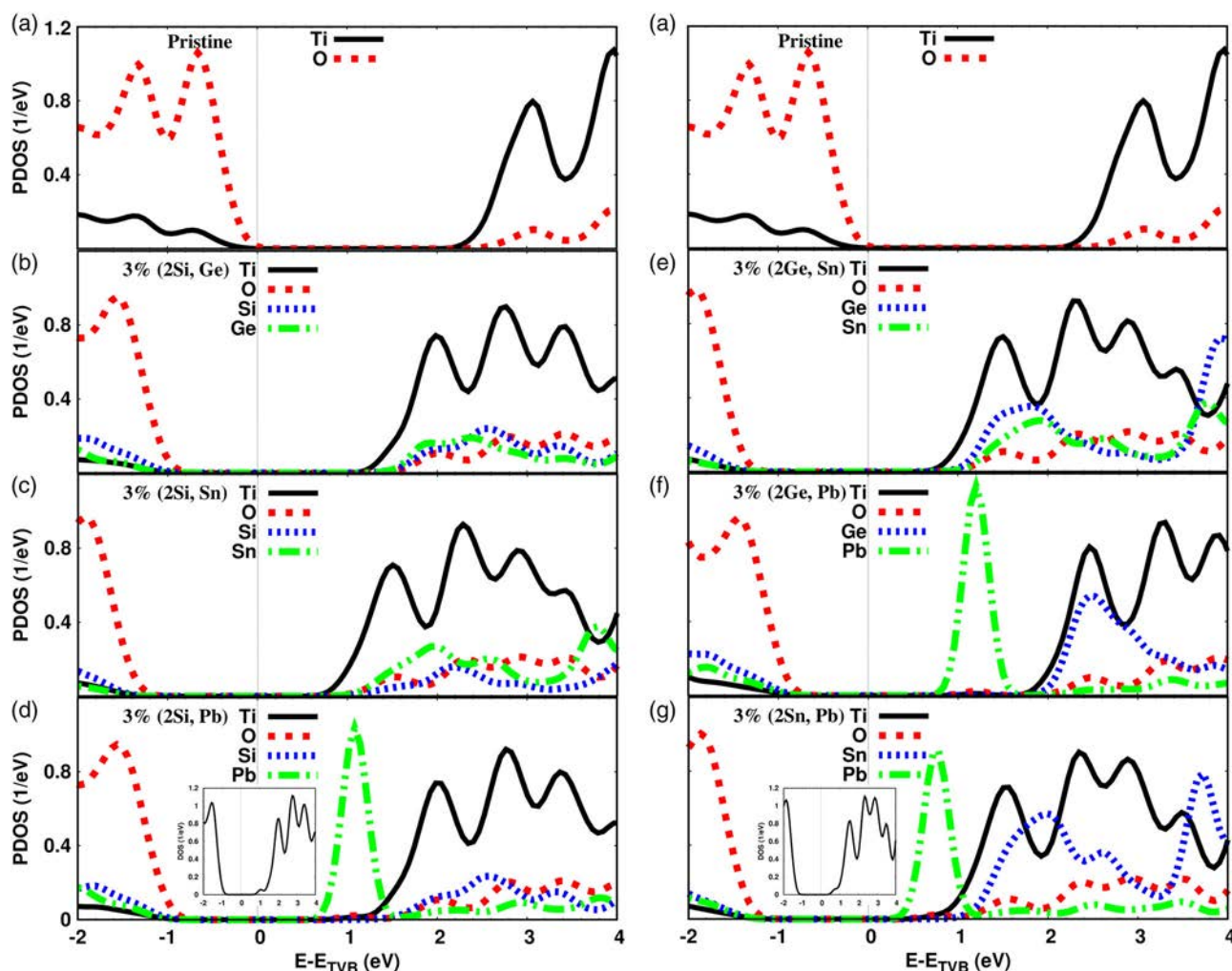
Figure 6. PDOS for a) pristine TNT, and for 3% co-doping: b) (2Si, Ge), c) (2Si, Sn), d) (2Si, Pb), e) (2Ge, Sn), f) (2Ge, Pb), and g) (2Sn, Pb). The (Ti, O) states are scaled down by a factor of 50 to allow easy comparison. The energy is given relative to the TVB of the pristine TNT. The insets in (d) and (g) show the corresponding total DOS.

The overlap between CB and Pb states is most pronounced at 1.4 eV, which results in a small shoulder in the DOS (see the inset of figure). This reduces the bandgap to 1.44 eV, less than the corresponding one for 2% co-doping but equal to the bandgap of 3% Pb mono-doping. The PDOSs of (Si, 2Pb) show the same gap and DOS shape as (Si, Pb) due to the dominant effect of the Pb states.

For (2Ge, Sn)/(Ge, 2Sn) co-doping (Figure 6e), the PDOSs are very similar to the case of (2Si, Sn) (Figure 6c) with a small shift of bands to higher energy. The bandgap is 1.86 eV, the same as for Ge mono-doping at any concentration. The PDOSs of (2Ge, Pb)/(Ge, 2Pb) are the same as for (Ge, Pb), with the same bandgap. The last 3% co-doped structure is (2Sn, Pb): as compared with the (2Si, Pb) system, the PDOS is very similar with respect to the Pb contribution, but there is a shift in energy due to the Sn states (in comparison with the Si states), consistent with what we observed for the case of Sn versus Si mono-doping. As compared with (Sn, Pb) co-doping, the CB and Pb states for (2Sn, Pb) are lower in energy due to the higher concentration of

Sn; the bandgap is 1.50 eV. For (Sn, 2Pb), due to the high concentration of Pb, the PDOS is similar to (Sn, Pb). The bandgaps of the 3% co-doped structures are also presented in Table 2.

We note that for a given co-doped system, say (2X, Y), there are different possibilities to position the X and Y atoms. We have considered such different cases, and we have confirmed that the DOSs are not affected.

4. Optical Properties

The optical properties of a semiconductor photocatalyst are closely related to its electronic structure. The decrease in the bandgap for all mono-dopants as compared with pristine TNT (see Figure 3) leads to a redshift of the optical absorption edge. This redshift depends on the kind of dopant and the concentration. Clearly, several factors are relevant for the differences between doped bulk TiO_2 and doped TNTs, namely, the geometry, electronic structure, and the interaction between

ADVANCED SCIENCE NEWS
www.advancedsciencenews.com

pss b
physica status solidi b
www.pss-b.com

dopant and neighboring Ti and O atoms, with the general tendency of reducing the optical gap. As is apparent from Figure 4, this leads to a shift of the absorption edge toward higher wavelengths, most pronounced for Pb mono- and (2Pb, Ge) co-doping.

In contrast, a reduction of the optical gap upon doping in the bulk system is only found for Si and Ge doping.[43] Our results agree qualitatively with the recently observed gap reduction for Sn-doped TNTs.[35]

The optical absorption is related to the complex dielectric function $\varepsilon(\omega) = \varepsilon_1(\omega) + i\varepsilon_2(\omega)$, with ω is the frequency. The imaginary part is calculated from the momentum matrix elements between the occupied and unoccupied states, and the real part is subsequently from the Kramers–Kronig relation. The absorption coefficient is then given by[60]

$$\alpha(\omega) = \sqrt{2}\omega\sqrt{\sqrt{\varepsilon_1^2(\omega) + \varepsilon_2^2(\omega)} - \varepsilon_1(\omega)}. \qquad (2)$$

A "scissors operation"[61–63] of 1.0 eV, which corresponds to the difference between the calculated and the experimental gap (3.2 eV) for pristine TNT, is also used for the doped system.

As a side remark, we wish to add that this "operation"— adding ad hoc a correction Δ to the conduction band energies, such that the calculated energy gap plus Δ (here, 1.0 eV) equals the experimental gap, is pretty much standard. It relates to the well-known problem of DFT that the gap calculated from the Kohn–Sham orbitals almost always is by far too small.[64,65] Another way out of this problem is to extend DFT and include so-called GW corrections, see the previous study[66] and references therein; but, this approach is computationally quite costly, and hence not practical for systematic studies of doped systems.

A pristine TNT can only absorb the narrow UV light (370 nm), but shows no absorption for visible light (see **Figure 7**). The calculated optical absorption spectra for all mono-doped TNTs show absorption in the visible-light region, namely, in the range of 380–410 nm. Also, a redshift is apparent for all mono-doped TNTs, consistent with the earlier discussion.

5. Application: Water Splitting

The improvement of the visible light activity of TiO$_2$ is very important for water splitting (H production).[67,68] In this context, it is important to note that the absolute values of the conduction and valence band edges, E_{CBE} and E_{VBE}, are required. This issue has been discussed extensively in the literature; see, e.g., the
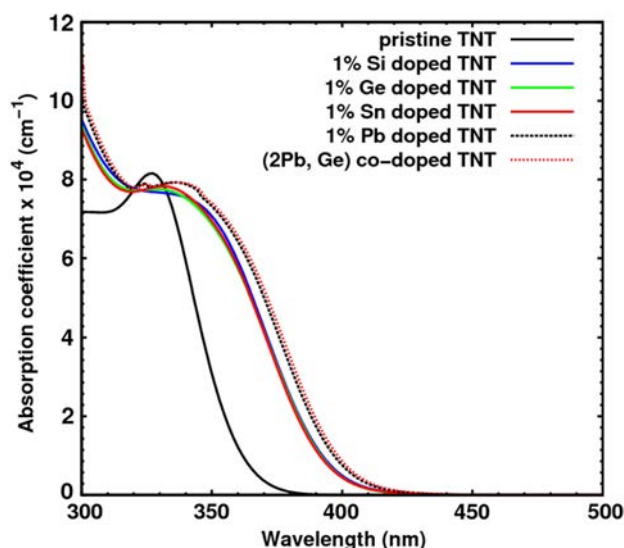

Figure 7. Absorption coefficients of pristine and mono- and co-doped TNTs.

study given by Grätzel,[10] or, more recently, the study given by Wang et al.[69] In short,[40] the conduction band edge is computed from the empirical relation $E_{CBE} = \overline{X} - 0.5E_{gap} - 4.5$ eV, where $\overline{X}$ denotes the geometric mean of the electronegativities of the constituents (e.g., $\overline{X} = (\chi_{Ti}\chi_O^2)^{1/3} = 5.80$ eV for the pristine case, using experimental values[70–72]), and E_{gap} is the scissors-corrected energy gap. Then, $E_{VBE} = E_{CBE} + E_{gap}$. Calculations of the conduction band edge (CBE) and the valence band edge (VBE) have shown that the CBE of anatase TiO$_2$ is located at -0.29 eV, and the VBE at 2.91 eV.[73] Note that these band edges are measured with respect to the normal hydrogen electrode (NHE) potential of the reduction and oxidation levels of water: the reduction level (H$^+$/H$_2$) is located at 0 eV, and the oxidation level (H$_2$O/O$_2$) at 1.23 eV. Thus, the CBE is "above" the water reduction (H$^+$/H$_2$) level, and the VBE is "below" the water oxidation (H$_2$O/O$_2$) level, in the standard representation.[10]

Table 3 shows that Si, Ge, and Sn mono-doping of TNTs improves the photocatalytic properties, at any concentration. However, the CBE value is too high compared with the reduction level of water; hence, Pb-doped TNTs are useful for hydrogen production despite the fact that they have the lowest bandgaps among the mono-dopants. The low-concentration Si- and Ge-doped structures show a better efficiency than for high concentration. In contrast, for bulk TiO$_2$ anatase, only Ge doping

Table 3. CBE and VBE, both in units of eV, of pristine TNT and doped TNTs for different concentrations. The energies are given with respect to the NHE potential; see the related discussion in Section 5 of the previous study.[40] Note that 0 eV (NHE) corresponds to -4.5 eV (vacuum). In the third row, the scissors-corrected energy gap, $E_{gap} = E_{VBE} - E_{CBE}$, is presented for completeness.

	pristine	Si dopant			Ge dopant			Sn dopant			Pb dopant		
		1%	2%	3%	1%	2%	3%	1%	2%	3%	1%	2%	3%
CBE	−0.29	−0.08	−0.06	−0.07	−0.11	−0.09	−0.07	−0.11	−0.09	−0.06	0.04	0.08	0.12
VBE	2.91	2.72	2.74	2.79	2.75	2.77	2.79	2.75	2.74	2.77	2.60	2.58	2.65
E_{gap}	3.20	2.80	2.80	2.86	2.86	2.86	2.86	2.86	2.83	2.83	2.56	2.50	2.44

improves the photocatalytic properties.[43] We do not present the co-doping results here because all of them have CBEs around −2 eV, which is higher than the reduction level of water, and the VBEs are higher than the oxidation level.

6. Summary

DFT has been used to study the structural, electronic, and optical properties of cation mono- and co-doped TNTs at different doping concentrations. All mono-/co-dopants, except (Sn, Ge) co-doping, decrease the bandgap of the TNT, similar to previous results.[40] For mono-dopants, Pb-doped TNTs have the lowest bandgap at the studied concentrations (1% to 3%) due to the presence of distinct Pb states below the conduction band. The contribution of the dopant states in the conduction band increases as we move down the 4A group in the periodic table, i.e., from Si to Ge, Sn, and Pb. The decrease in the bandgaps of mono-doped TNTs is accompanied by shifts in the band edges toward lower energy for Si, Ge, and Sn. The bandgaps of 2% co-doped TNTs, except for (Ge, Sn), are smaller than those of Si, Ge, and Sn mono-doped TNTs at any concentration. The (Pb, 2X; $X =$ Si, Pb) co-doped TNTs have the lowest bandgap of all mono- and co-doped TNTs. However, (Ge, Sn) 2% co-doped TNT has the largest bandgap not only of all mono- and co-doped TNTs but also compared with the pristine nanotube. The influence of co-dopants can be understood, to a large extent, in terms of a superposition of individual mono-dopant effects. The study of optical properties illustrates that mono- and co-doped TNTs can absorb a wide range of visible light, in contrast to pristine TNT. This observation, consistent with recent experimental results, is related to the decrease in the bandgap. The Si, Ge, and Sn mono-doped TNTs at low concentration (1%) have a high ability to produce hydrogen in the water splitting process, their performance being clearly better than for pristine TNT. The energetic locations of the bandgap edges of Pb mono-doped and co-doped TNTs, however, prevent their use for this application.

7. Computational Details

We applied DFT using the GGA[66] and the Perdew–Burke–Ernzerhof functional[74] as implemented in the SIESTA package.[75] (Generally speaking, the accuracy of DFT-GGA calculations—which notoriously underestimate the bandgap—is always an issue. In this context, we mention that this question was thoroughly discussed in a recent paper,[66] with the conclusion that DFT-GGA is "an empirical, yet practical" approach. See also previous studies[61–63] in relation to the "scissors operation".) The wave functions were expanded using a local atomic orbitals basis set; the energy cutoff was 300 Ry, and the Monkhorst–Pack k-meshes contained $1 \times 1 \times 12$ points. Structural relaxation was carried out with the conjugate gradient method until the net force on every atom was smaller than 0.04 eV Å^{-1}. As we were interested in the properties of nanotubes, a rectangular supercell, $20 \times 20 \times L$ Å^3, was used, where L is the length of the nanotube along the z axis. The distance between two neighboring TNTs, in x and y directions, was thus 20 Å, which was sufficient to avoid any image interaction. Test calculations, changing the size of the supercell and the number of k points, showed the convergence of our results. In particular, to check for the spurious dipole–dipole interaction between image supercells, the cell was increased to $30 \times 30 \times L$ Å^3; however, no effect was observed. (This aspect is discussed in detail, e.g., in Refs. [76,77].) Spin polarized calculations were also performed for selected systems, but no modifications were found.

Conflict of Interest

The authors declare no conflict of interest.

[1] T. Tachikawa, T. Majima, *Chem. Soc. Rev.* **2010**, *39*, 4802.
[2] C. C. Chen, W. H. Ma, J. C. Zhao, *Chem. Soc. Rev.* **2010**, *39*, 4206.
[3] F. Spadavecchia, G. Cappelletti, S. Ardizzone, M. Ceotto, L. Falciola, *J. Phys. Chem. C* **2011**, *115*, 6381.
[4] A. Motonari, J. Jinting, I. Seiji, *Curr. Nanosci.* **2007**, *3*, 285.
[5] D. Deng, M. G. Kim, J. Y. Lee, J. Cho, *Energy Environ. Sci* **2009**, *2*, 818.
[6] T. Umebayashi, T. Yamaki, H. Itoh, K. Asai, *Appl. Phys. Lett.* **2002**, *81*, 454.
[7] L. Y. Mu, J. J. Hyun, A. J. Hyung, J. Y. Sun, J. K. Ok, H. K. Seog, K. B. Hoon, *Proc. Res. J. Cer.* **2005**, *6*, 302.
[8] J. Zhao, X. Wang, T. Sun, L. Li, *Nanotechnology* **2005**, *16*, 2450.
[9] M. R. Hoffmann, S. T. Martin, W. Choi, D. W. Bahnemann, *Chem. Rev.* **1995**, *95*, 69.
[10] M. Grätzel, *Nature* **2001**, *414*, 338.
[11] O. K. Varghese, D. Gong, M. Paulose, K. G. Ong, E. C. Dickey, C. A. Grimes, *Adv. Mater.* **2003**, *15*, 624.
[12] V. Narayanamurti, *Physics Today* **1984**, *37*, 24.
[13] F. Capasso, *Science* **1987**, *235*, 172.
[14] Y. Q. Wang, G. Q. Hu, X. F. Duan, H. L. Sun, Q. K. Xue, *Chem. Phys. Lett.* **2002**, *365*, 427.
[15] D. V. Potapenko, J. Hrbek, R. M. Osgood, *ACS Nano* **2008**, *2*, 1353.
[16] J. Biener, E. Farfan-Arribas, M. Biener, C. M. Friend, R. J. Madix, *J. Chem. Phys.* **2005**, *123*, 094705.
[17] B. Liu, J. E. Boercker, E. S. Aydil, *Nanotechnology* **2008**, *19*, 505604.
[18] Y. J. Hwang, A. Boukai, P. Yang, *Nano Lett.* **2009**, *9*, 410.
[19] P. Hoyer, *Langmuir* **1996**, *12*, 1411.
[20] S. P. Albu, A. Ghicov, J. M. Macak, R. Hahn, P. Schmuki, *Nano Lett.* **2007**, *7*, 1286.
[21] G. K. Mor, K. Shankar, M. Paulose, O. K. Varghese, C. A. Grimes, *Nano Lett.* **2005**, *5*, 191.
[22] G. K. Mor, O. K. Varghese, R. H. T. Wilke, S. Sharma, K. Shankar, T. J. Latempa, K. S. Choi, C. A. Grimes, *Nano Lett.* **2008**, *8*, 1906.
[23] M. A. Khan, O. B. Yang, *Catal. Today* **2009**, *146*, 177.
[24] A. N. Enyashin, G. Seifert, *Phys. Status Solidi B* **2005**, *242*, 1361.
[25] A. M. Ferrari, D. Szieberth, M. Claudio, Z. Wilson, R. Demichelis, *J. Phys. Chem. Lett.* **2010**, *1*, 2854.
[26] D. Szieberth, A. M. Ferrari, Y. Noel, M. Ferrabone, *Nanoscale* **2010**, *2*, 81.
[27] R. A. Evarestov, A. V. Bandura, M. V. Losev, S. Piskunov, Y. F. Zhukovskii, *Physica E* **2010**, *43*, 266.
[28] A. V. Bandura, R. A. Evarestov, *Surf. Sci.* **2009**, *603*, L117.

[29] O. K. Varghese, D. Gong, M. Paulose, C. A. Grimes, E. C. Dickey, *J. Mater. Res.* **2003**, *18*, 156.

[30] F. Cesano, S. Bertarione, A. Damin, G. Agostini, S. Usseglio, J. G. Vitillo, C. Lamberti, G. Spoto, D. Scarano, A. Zecchina, *Adv. Mater.* **2008**, *20*, 3342.

[31] G. Wang, H. Feng, L. Hu, W. Jin, Q. Hao, A. Gao, X. Peng, W. Li, K.-Y. Wong, H. Wang, Z. Li, P. K. Chu, *Nat. Commun.* **2018**, *9*, 2055.

[32] D.-D. Qin, Q.-H. Wang, J. Chen, C.-H. He, Y. Li, C.-H. Wang, J.-J. Quan, C.-L. Tao, X.-Q. Lu, *Sust. Energy Fuels* **2017**, *1*, 248.

[33] Y. Yang, L. C. Kao, Y. Liu, K. Sun, H. Yu, J. Guo, S. Y. H. Liou, M. R. Hoffmann, *ACS Catal.* **2018**, *8*, 4278.

[34] Z. Dong, D. Ding, T. Li, C. Ning, *RSC Adv.* **2018**, *8*, 5652.

[35] J. Li, X. Xu, X. Liu, C. Yu, D. Yan, Z. Sun, L. Pan, *J. Alloys Compd.* **2016**, *679*, 454.

[36] A. Chatzitakis, M. Grandcolas, K. Xu, S. Mei, J. Yang, I. J. T. Jensen, C. Simon, T. Norby, *Catal. Today* **2017**, *287*, 161.

[37] D. J. Mowbray, J. I. Martinez, J. M. G. Lastra, K. S. Thygesen, K. W. Jacobsen, *J. Phys. Chem. C* **2009**, *113*, 12301.

[38] S. Piskunov, O. Lisovski, J. Begens, D. Bocharov, Y. F. Zhukovskii, M. Wessel, E. Spohr, *J. Phys. Chem. C* **2015**, *119*, 18686.

[39] A. Chesnokov, O. Lisovski, D. Bocharov, S. Piskunov, Y. F. Zhukovskii, M. Wessel, E. Spohr, *Phys. Scr.* **2015**, *90*, 094013.

[40] M. M. Fadlallah, *Physica E* **2017**, *89*, 50.

[41] S.-M. Oh, S. S. Kim, J. E. Lee, T. Ishigaki, D.-W. Park, *Thin Solid Films* **2003**, *435*, 252.

[42] H. Ozaki, S. Iwamoto, M. Inoue, *Chem. Lett.* **2005**, *34*, 1082.

[43] R. Long, Y. Dai, G. Meng, B. Huang, *Phys. Chem. Chem. Phys.* **2009**, *11*, 8165.

[44] K. S. Yang, Y. Dai, B. B. Huang, *Chem. Phys. Lett.* **2008**, *456*, 71.

[45] Y. Duan, N. Fu, Q. Liu, Y. Fang, X. Zhou, J. Zhang, Y. Lin, *J. Phys. Chem. C* **2012**, *116*, 8888.

[46] M. Sun, X. Zhang, J. Li, X. Cui, D. Sun, Y. Lin, *Electrochem. Commun.* **2012**, *16*, 26.

[47] E. Arpaç, F. Sayılkan, M. Asiltürk, P. Tatar, N. Kiraz, H. Sayılkan, *J. Hazard. Mater.* **2007**, *140*, 69.

[48] J. Yu, J. C. Yu, B. Cheng, X. Zhao, *J. Sol-Gel Sci. Tech.* **2002**, *24*, 39.

[49] Y. J. Zhou, F. He, J. G. Qi, Y. Wang, *Adv. Mater. Res.* **2011**, *299-300*, 558.

[50] J. Xiao, Z. Pan, B. Zhang, G. Liu, H. Zhang, X. Song, G. Hu, C. Xiao, Z. Wei, Y. Zheng, *Mater. Lett.* **2017**, *188*, 66.

[51] M. Grätzel, *Acc. Chem. Res.* **2009**, *42*, 1788.

[52] F. Nunzi, F. De Angelis, *J. Phys. Chem. C* **2011**, *115*, 2179.

[53] L. Deng, Y. Chen, M. Yao, S. Wang, B. Zhu, W. Huang, S. Zhang, *J. Sol-Gel Sci. Technol.* **2010**, *53*, 535.

[54] A. Shyichuk, G. Meinrath, S. Lis, *J. Rare Earths* **2016**, *34*, 820.

[55] Z. Zhao, Q. Liu, *J. Phys. D: Appl. Phys.* **2008**, *41*, 085417.

[56] C. G. V. de Walle, J. Neugebauer, *J. Appl. Phys.* **2004**, *95*, 3851.

[57] M. M. Momeni, Z. Nazari, *Ceram. Int.* **2016**, *42*, 8691.

[58] M. M. Momeni, Y. Ghayeb, *J. Electroanal. Chem.* **2015**, *751*, 43.

[59] Y. Su, S. Chen, X. Quan, H. Zhao, Y. Zhang, *Appl. Surf. Sci.* **2008**, *255*, 2167.

[60] M. Bass, E. W. V. Stryland, D. R. Williams, W. L. Woffe, *Handbook of Optics*, 2nd ed., vol. 1, McGraw-Hill, New York **1995**.

[61] H. Weng, J. Dong, T. Fukumura, M. Kawasaki, Y. Kawazoe, *Phys. Rev. B* **2006**, *73*, 121201(R).

[62] F. H. Tian, C. B. Liu, *J. Phys. Chem. B* **2006**, *110*, 17866.

[63] X. Zhang, M. Guo, W. Li, C. Liu, *J. Appl. Phys.* **2008**, *103*, 063721.

[64] C. S. Wang, B. M. Klein, *Phys. Rev. B* **1981**, *24*, 3417.

[65] R. W. Godby, M. Schlüter, L. J. Sham, *Phys. Rev. B* **1988**, *37*, 10159.

[66] Á. Morales-García, R. Valero, F. Illas, *J. Phys. Chem. C* **2017**, *121*, 18862.

[67] X. Chen, S. Shen, L. Guo, S. S. Mao, *Chem. Rev.* **2010**, *110*, 6503.

[68] B. Modak, S. K. Ghosh, *J. Phys. Chem. C* **2015**, *119*, 23503.

[69] G.-Z. Wang, H. Chen, G. Wu, A.-L. Kuang, H.-K. Yuan, *Chem. Phys. Chem.* **2016**, *17*, 489.

[70] M. V. Putz, N. Russo, E. Sicilia, *Theor. Chem. Acc.* **2005**, *114*, 38.

[71] E. C. M. Chen, W. E. Wentworth, *J. Chem. Edu.* **1975**, *52*, 486.

[72] *CRC Handbook of Chemistry and Physics*, 84th ed. (Ed: D. R. Lide), CRC Press, Boca Raton **2003**.

[73] Y. Xu, M. A. A. Schoonen, *Am. Mineral.* **2000**, *85*, 543.

[74] J. P. Perdew, K. Burke, M. Ernzerhof, *Phys. Rev. Lett.* **1996**, *77*, 3865.

[75] J. M. Soler, E. Artacho, J. D. Gale, A. García, J. Junquera, P. Ordejón, D. Sánchez-Portal, *J. Phys.: Condens. Matter* **2002**, *14*, 2745.

[76] A. M. Souza, I. Rungger, C. D. Pemmaraju, U. Schwingenschlögl, S. Sanvito, *Phys. Rev. B* **2013**, *88*, 165112.

[77] M. J. Rutter, *J. Phys.: Condens. Matter* **2019**, *31*, 335901.

1900217 (11 of 11)